Soil Biology and Biochemistry 178 (2023) 108921

Contents lists available at ScienceDirect

Soil Biology and Biochemistry

journal homepage: www.elsevier.com/locate/soilbio

# Microscale spatial distribution and soil organic matter persistence in top and subsoil

Thiago M. Inagaki [a,d,g,*], Angela R. Possinger [b,1], Steffen A. Schweizer [a], Carsten W. Mueller [a,e], Carmen Hoeschen [a], Michael J. Zachman [c,2], Lena F. Kourkoutis [c,f], Ingrid Kögel-Knabner [a,d], Johannes Lehmann [b,d]

[a] TUM School of Life Sciences, Technical University of Munich, Emil-Ramann-Straße 2, Freising, 85354, Germany
[b] Soil and Crop Sciences, Cornell University, 909 Bradfield Hall, Ithaca, NY, 14853, USA
[c] School of Applied and Engineering Physics, 271 Clark Hall, Cornell University, Ithaca, NY, 14853, USA
[d] Institute for Advanced Study, Technical University of Munich, Lichtenbergstraße 2a Garching, 85748, Germany
[e] Department of Geosciences and Natural Resource Management, University of Copenhagen, Øster Voldgade 10, DK-1350, Copenhagen K, Denmark
[f] Kavli Institute at Cornell for Nanoscale Science, Cornell University, Ithaca, NY, 14853, USA
[g] Department of Biogeochemistry and Soil Quality, Norwegian Institute of Bioeconomy Research (NIBIO), Høgskoleveien 7, 1430 Ås, Norway

ARTICLE INFO

*Keywords:*
Soil microbial community
Soil heterogeneity
Organo-mineral associations
NanoSIMS
FIB-SEM
Soil organic matter

ABSTRACT

The spatial distribution of organic substrates and microscale soil heterogeneity significantly influence organic matter (OM) persistence as constraints on OM accessibility to microorganisms. However, it is unclear how changes in OM spatial heterogeneity driven by factors such as soil depth affect the relative importance of substrate spatial distribution on OM persistence. This work evaluated the decomposition and persistence of $^{13}C$ and $^{15}N$ labeled water-extractable OM inputs over 50 days as either hotspot (i.e., pelleted in 1–2 mm-size pieces) or distributed (i.e., added as OM < 0.07 μm suspended in water) forms in topsoil (0–0.2 m) and subsoil (0.8–0.9 m) samples of an Andisol. We observed greater persistence of added C in the subsoil with distributed OM inputs relative to hotspot OM, indicated by a 17% reduction in cumulative mineralization of the added C and a 10% higher conversion to mineral-associated OM. A lower substrate availability potentially reduced mineralization due to OM dispersion throughout the soil. NanoSIMS (nanoscale secondary ion mass spectrometry) analysis identified organo-mineral associations on cross-sectioned aggregate interiors in the subsoil. On the other hand, in the topsoil, we did not observe significant differences in the persistence of OM, suggesting that the large amounts of particulate OM already present in the soil outweighed the influence of added OM spatial distribution. Here, we demonstrated under laboratory conditions that the spatial distribution of fresh OM input alone significantly affected the decomposition and persistence of OM inputs in the subsoil. On the other hand, spatial distribution seems to play a lower role in topsoils rich in particulate OM. The divergence in the influence of OM spatial distribution between the top and subsoil is likely driven by differences in soil mineralogy and OM composition.

## 1. Introduction

Soils represent an extensive carbon (C) reservoir and have a recognized role in food production, water quality, and biodiversity (Vermeulen et al., 2019). In the last few decades, soil organic carbon (SOC) sequestration has become more prominent in the debate on climate change mitigation (Rumpel et al., 2018). The persistence of organic matter (OM) inputs from aboveground and belowground sources is an essential factor regulating SOC storage (Lal et al., 2018). This process is now recognized as mediated by microorganisms, reinforcing that the most persistent OM first passes through the microbial biomass (Liang et al., 2019). Aboveground litter, rhizosphere, root exudates, and leachates of dissolved organic matter (DOM) stand out as main inputs of soil OM (Marin-Spiotta et al., 2011; Castellano et al., 2015; Baumert et al., 2018).

These substrates' spatial distribution and concentration vary in soil,

* Corresponding author. TUM School of Life Sciences, Technical University of Munich, Emil-Ramann-Straße 2, Freising, 85354, Germany.
*E-mail address:* thiago.inagaki@nibio.no (T.M. Inagaki).
[1] Current address: School of Plant and Environmental Sciences, Virginia Tech, Blacksburg, VA 24061, USA.
[2] Current address: Center for Nanophase Materials Sciences, Oak Ridge National Laboratory, Oak Ridge, TN 37831, USA.

https://doi.org/10.1016/j.soilbio.2022.108921
Received 7 March 2022; Received in revised form 16 December 2022; Accepted 17 December 2022
Available online 22 December 2022

ranging from highly concentrated hotspots (e.g., rhizosphere and plant residues) (Marschner et al., 2012; Kuzyakov and Blagodatskaya, 2015) to distributed sources at low concentrations (e.g., DOM in leachate) (Marschner and Kalbitz, 2003). It is well recognized that the spatial distribution of soil OM significantly affects its persistence in the soil since it directly affects OM accessibility to microorganisms (Kuka et al., 2007; Wagai et al., 2013; Nunan et al., 2017; Shi et al., 2021b). Contact between decomposing organisms and their enzymes with an OM substrate is necessary for decomposition in soils, making substrate availability a key factor for SOC turnover (Ebrahimi and Or, 2018). Microorganisms such as soil bacteria and other prokaryotes are conservative in moving toward their food since it requires large amounts of energy, and any distance could reduce their efficiency in promoting decomposition (Van Haastert and Bosgraaf, 2009; Reynolds et al., 2010; Nunan et al., 2020). Thus, soil spatial heterogeneity has been proposed as a reason for limited decomposition, reducing the colocalization between the substrate and decomposers (Falconer et al., 2015; Nunan et al., 2017; Lehmann et al., 2020; Shi et al., 2021b). Although many studies have evaluated the influence of spatial heterogeneity on microorganism behavior through modeling techniques (Van Veen and Kuikman, 1990; Abu-Ashour et al., 1994; Kuka et al., 2007; Babey et al., 2017; Baveye et al., 2018; Vogel et al., 2018; Nunan et al., 2020), few investigations have experimentally evaluated the direct effect of the spatial distribution of the OM input on its persistence (e.g., in hotspot or distributed forms), particularly in the context of variation in spatial and chemical properties of the soil organo-mineral matrix at the microscale. Overall, more experimental evidence of how spatial distribution alone regulates OM turnover in soils is needed to improve our understanding of model assumptions.

Soil spatial heterogeneity at the microscale and mechanisms driving OM persistence can vary widely among soils due to mineral properties, degree of weathering, and parent materials (Kögel-Knabner and Amelung, 2020). Such variability can also be observed with soil depth. While organic fractions of particulate OM have been recognized as important agents for OM stabilization, especially in the topsoil (Tisdall and Oades, 1982; Besnard et al., 1996; Witzgall et al., 2021), organo-mineral associations with Fe and Al (hydro)oxides have been highlighted as significant mechanisms in subsoils (Rumpel and Kögel-Knabner, 2010; Marin-Spiotta et al., 2011; Inagaki et al., 2020; Wagai et al., 2020). However, it is still poorly understood how the spatial distribution of OM can influence the partitioning between these different pools.

Here, we investigated the mineralization and persistence of a water-extractable OM input varying only in its spatial distribution (hotspot vs. distributed) in an Andisol (topsoil 0–0.2 m and subsoil 0.8–0.9 m). We use the term "mineralization" to refer to the conversion of organic carbon to $CO_2$ and water, as defined by Vert et al. (2012). Also, we use the term "persistence" to refer to reduced OM mineralization and "decomposition" to refer to the transformation of organic material. We hypothesized that spatial distribution alone could increase the persistence of distributed OM inputs compared to substrate concentrated in hotspots due to lower accessibility to microorganisms. We assumed that greater allocation of OM to the mineral-associated pool contributes to increased persistence. We also hypothesized that the influence of spatial distribution could vary according to soil depth due to differences in mineralogical properties.

## 2. Material and methods

### 2.1. Soil samples, experimental design, and $^{13}C$ and $^{15}N$ enriched substrate

This study used two Andisol soil samples from the top (0–0.2 m) and subsoil (0.8–0.9 m) depths. The samples were collected in mixed fern vegetation (hapu'u – *Cybotium* spp.- and uluhe – *Dicronopteris linearis* Burm.) at the Kohala region – Hawaii (20°4′14.16" N, 155°43′21.94" E). The soil is classified as an Andisol (Soil Survey Staff, 2010) derived from alkalic lavas of the 350 ka Pololu basalt. These soils likely also received ash deposition from the younger (150 ka) Hawi basalt series (Wolfe and Morris, 1996). The samples were air-dried and separated for the lab incubations. Details of soil sampling protocols are described in Grant et al. (2019), Kramer et al. (2012), and Schoeneberger et al. (2012).

The $^{13}C$ labeled water-extractable OM used as a substrate in our experiment was extracted from shrub willow leaves enriched with $^{13}CO_2$ (*Salix viminalis x S. miyabeana*). A detailed description of plant cultivation can be found in DeCiucies et al. (2018). Briefly, the willow leaves were sieved with a 2 mm sieve and shaken in deionized water (leaves/water proportion of 1:10) for 72 h at 32 °C with an orbital shaker at 100 rpm. After the shaking, the suspension was filtered with a Whatman glass microfiber filter of 0.7 μm. The solution that passed through the filter was then freeze-dried.

Two treatments with contrasting spatial distributions were produced with this water-extractable OM: "hotspot" (1–2 mm size pellets); and "distributed" (colloidal suspended material filtered to 0.7 μm) (Supplementary Fig. 2). For producing the "hotspot OM" form, we pressed the freeze-dried extracted OM using a hydraulic press to form solid pieces. Then, we cracked the compressed material into 1–2 mm pieces and mixed them with the soil for incubation. To produce the "distributed OM," we dissolved the freeze-dried OM into deionized water and mixed the OM solution into the soil for incubation. The $^{13}C$ enrichment levels of the amendments were 1.77 atom percentages for the willow hotspot OM and distributed OM. The $^{15}N$ enrichment levels were 7.59 and 7.62 atom percentages for the hotspot OM and distributed OM, respectively (Supplementary Fig. 2).

The incubation experiment design was completely randomized with three replicates. We used soil samples from two depths: 0–0.2 m and 0.8–0.9 m, as representative samples of the A and B horizons. For each depth, we added $^{13}C$ and $^{15}N$ labeled amendments as follows: 1) control: incubated soil without amendment and OM in two different forms: 2) hotspot (1–2 mm size pellets), and 3) distributed (colloidal particles filtered at 0.7 μm) (Supplementary Fig. 2). We emphasize that our organic matter input contains particles 0.25 μm bigger than what is operationally defined as "dissolved OM" in soil (i.e., particles <0.45 μm) (Thurman, 2012). Because the objective of our experiment is to verify the influence of OM spatial distribution (hotspot vs. distributed), the inclusion of particles between 0.45 and 0.7 μm does not interfere with our interpretations.

### 2.2. Incubation experiment

For the incubation, we standardized the amendment inputs to 10 mg C g soil$^{-1}$. The carbon input rate was similar to overall biomass-C inputs in Hawaiian forests (Ostertag et al., 2009). This C concentration was selected to provide sufficient OM levels for the detection of both added and native soil OM in subsequent imaging and isotope analysis, in line with the main goal of this mechanistic experiment to test the influence of OM spatial distribution on C persistence. All the soil + amendment samples were maintained at 50% of the water holding capacity, according to Lowery et al. (1997). Pre-tests with topsoil and subsoil samples were performed to obtain the water amount necessary to reach the desired water hold capacity. The samples were added to 60 mL Qorpak bottles with 3 g of soil + amendment mixture. The amount of soil used was restricted not to surpass the limits of $CO_2$ detection by the gas analyzer. The soils and hotspot OM inputs were gently turned around 10 times by hand to provide a homogeneous mixture in a dry state. The water was then added with a pipette to reach the desired moisture level. For the distributed OM input, we mixed the freeze-dried <0.7 μm OM in the water used to reach the desired moisture level. The input was then added to the water in the soil with a pipette.

The Qorpak bottle was placed in a 1 L Mason jar containing 10 mL of water to maintain 100% humidity. All the samples were incubated for 50 days. We used a Picarro $CO_2$ stable isotope analyzer (G2201-I, Santa Clara, CA, USA) to monitor the incubation continuously. Each jar's

headspace gas was sampled, and $CO_2$ concentration was measured along with $^{13}C$ for 6 min during each sampling period and purged with $CO_2$-free air. We collected the data at a rate of two measurements per second over the sampling time, and during the sample purge phase, we recorded the baseline values (i.e., blank values) before each cycle's mineralization measurement. Mineralization rates were measured every 10 h. The soils were air-dried after incubation, and soil OM fractionation was performed.

### 2.3. Samples characterizations and soil organic matter fractionation

#### 2.3.1. Top and subsoil samples characterization

Before and after the incubation, we performed soil OM fractionation of samples from the top and subsoil used as the base of this experiment. The procedure was adapted from the method of Golchin et al. (1994). Briefly, the soil was mixed in a proportion of 1: 2.5 (soil/solution) with a dense solution of sodium polytungstate at 1.8 g $cm^{-3}$. After standing overnight, we separated the floating free particulate organic matter (fPOM) using an electrical pump.

The soil suspension was then sonicated with an energy input of 1500 J $mL^{-1}$ using an ultrasonic disperser (SonopulsHD2200, Bandelin, Berlin – Germany). The chosen energy level is considered sufficient for the dispersion of the highly stable Andisol microaggregates without causing damage to the primary mineral structure (Silva et al., 2015). After the sonication period, the soil suspension was centrifuged (8500 g, 40 min), and the floating occluded particulate organic matter (oPOM) was separated using an electrical pump.

The mineral soil at the bottom of the centrifuge tube was then sieved using a 20 μm mesh sieve to separate sand and coarse silt fraction. The soil that passed through the sieve was then subjected to sedimentation and divided into two size fractions of 20–2 μm and <2 μm. All the fractions were rinsed until the electrical conductivity dropped 10 μS $cm^{-1}$ and freeze-dried. The C and N contents were measured by dry combustion using a CN elemental analyzer (CHNSO Elemental Analyzer, Hekatech, Wegberg – Germany). At least 97% of the C and N contents were recovered for all the samples fractionated.

The fractionation revealed that topsoil samples were composed of approximately 80% of particulate organic matter (fPOM and oPOM), while the subsoil was composed of approximately 95% mineral soil (20–2 and <2 μm). In both depths, the sand and coarse silt fraction were present in a low amount (less than 1% of total C) (Supplementary Fig. 1). Therefore, the fractionation procedure after the incubation only considered two fractions below and above 1.8 mg $cm^{-3}$ of density, here named the light and heavy fraction, respectively.

We also performed Fe and Al extractions using dithionite citrate bicarbonate (DCB) and ammonium oxalate (OX) in parallel samples using the methods described by Mehra and Jackson (1958), respectively. We measured soil pH on 0.01 M $CaCl_2$ using a pH meter (Orion Star A111, ThermoFisher Scientific, Waltham – MA, USA) and exchangeable Ca, Mg, and K using the $NH_4OAc$ method at pH 7 (Lavkulich, 1981). The extracted elements were measured by inductively coupled plasma optical emission spectroscopy (ICP-OES) (Vista-Pro CCD simultaneous, Varian, Darmstadt - Germany). The soil properties of the top and subsoil samples used in the experiment are described in Table 1.

#### 2.3.2. Soil organic matter characterization by $^{13}C$ CP/MAS NMR spectroscopy

The light and heavy fractions of top and subsoil samples used for the incubation experiment and the OM amendments were analyzed by $^{13}C$ CP/MAS NMR spectroscopy (Biospin DSX 200 NMR spectrometer, Bruker, Rheinstetten, Germany) for OM characterization (Supplementary Fig. 3). We used a contact time of 0.001 s with a pulse delay of 0.4 s for the heavy fraction and 1 s for the light fraction. At least 100,000 accumulated scans were performed to obtain a well-resolved spectrum. The spectra were integrated using four major chemical shift regions: 0–45 ppm (alkyl-C), 45–110 ppm (O/N-alkyl-C), 110 to 160 (aryl-C), and 160–220 ppm (carboxyl-C) (Knicker and Ludemann, 1995). Despite the high Fe content of the heavy fraction, it was not necessary to perform a pre-treatment with hydrofluoric acid to obtain a well-resolved spectrum.

**Table 1**
**Characterization of the topsoil and subsoil bulk samples used in the incubation experiment.** C and N contents, Fe and Al extractions, soil pH, nutrient content, and specific surface area.

| Analysis | Soil depth (m) | |
|---|---|---|
| | 0–0.2 | 0.8–0.9 |
| SOC content (mg $g^{-1}$) | 332.15 | 132.45 |
| N content (mg $g^{-1}$) | 1.15 | 0.36 |
| pH ($CaCl_2$) | 3.40 | 4.40 |
| Fe OX (mg $g^{-1}$) | 12.54 | 79.93 |
| Al OX (mg $g^{-1}$) | 2.02 | 107.71 |
| Fe DCB (mg $g^{-1}$) | 42.02 | 118.66 |
| Al DCB (mg $g^{-1}$) | 4.00 | 52.95 |
| Ca (mmol $g^{-1}$) | 0.44 | 0.00 |
| Mg (mmol $g^{-1}$) | 0.21 | 0.02 |
| K (mmol $g^{-1}$) | 0.05 | 0.02 |
| SSA ($m^2$ $g^{-1}$) | 3.43 | 53.35 |

SOC: soil organic carbon; OX: ammonium oxalate extracted; DCB: dithionite citrate bicarbonate extracted; SSA: specific surface area.

### 2.4. Aggregate cross-sectioning and NanoSIMS analysis

To evaluate the OM distribution and permeation of the labeled OM in the soil, we performed cross-sectioning of air-dried soil aggregates embedded with epoxy resin according to the method described by Mueller et al. (2013). We randomly selected macroaggregates of approximately 2 mm in size, embedded them in epoxy resin, and ground them down until approximately half using a 1 μm grade sandpaper. We then analyzed the polished sections with reflected light microscopy (Axio Imager Z2, Zeiss, Germany) and scanning electron microscopy (JSM 5900LV, JEOL, Japan). We hypothesized that infiltration through the soil pore system would be the main pathway of organic matter entrance into the soil macroaggregates. Therefore, we selected regions of interest at the interfaces of the pore system (i.e., the space through which the resin has infiltrated during the embedding) and the soil mineral surfaces. We analyzed the element and isotope distributions of the regions of interest using nanoscale secondary ion mass spectrometry (NanoSIMS 50 L, Cameca, France). The secondary ion collectors were used to measure the following ion species: $^{12}C^-$, $^{13}C^-$, $^{16}O^-$, $^{12}C^{14}N^-$, $^{12}C^{15}N^-$, $^{27}Al^{16}O^-$, and $^{56}Fe^{16}O^-$. The potential charging of surfaces was minimized using the internal electron flood gun. Before the measurement, the samples were coated with Au/Pd (~30 nm; SCD 005 sputter coater, Baltec GmbH, Germany). The NanoSIMS measurements were performed with a 30 μm field of view, 256 pixels dimensions, and 40 repeated scans of 1 ms. We have made four measurements in two macroaggregates for each treatment in top and subsoil samples, looking for "hot spots" of $^{12}C^{15}N$ enrichment. We opted to measure $^{15}N$ enrichments because the $^{13}C$ enrichment was too low to be detected in the NanoSIMS.

### 2.5. Multi-channel machine-learning segmentation and image analysis

The image analysis was conducted similarly to Inagaki et al. (2020) and Schweizer et al. (2018). Briefly, the electron multiplier dead time was corrected using the OpenMIMS plugin for ImageJ (Gormanns et al., 2012). After the auto-alignment of the scanning planes according to the $^{16}O^-$ distribution, the sum images of all ion species were computed. To quantify the spatial architecture of the soils, we performed two supervised pixel classifications based on the machine-learning algorithm using Ilastik 1.2 (Sommer et al., 2011). This image segmentation approach enables multiple image features like intensity, texture, and

gradient in all isotope distributions. Further details on the segmentation process are described by Schweizer et al. (2018). The first segmentation was performed with four-channel stack images including $^{16}O^-$, $^{12}C^- + ^{13}C^-$, $^{12}C^{14}N^- + ^{12}C^{15}N^-$ and $^{12}C^{15}N^-/(^{12}C^{14}N^- + ^{12}C^{15}N^-)$ (scaled to 0–5%) (Supplementary Fig. 4 b,c). The segmentation enabled us to distinguish material classes related to the spatial distribution of OM: resin 1 (high $C^-$), resin 2 (high $C^-$ and slightly elevated $CN^-$), mineral (high $O^-$), regions with low ion counts, OM (high $C^-$ and high $CN^-$) and $^{15}N$ enriched segments (high $^{15}N$ enrichment) (Supplementary Fig. 4d). The area contributions of mineral, OM, and $^{15}N$ enriched segments were compared according to their relative proportion of pixels. The mean $^{15}N$ enrichment of the OM and $^{15}N$ enriched segments was computed. An overall $^{15}N$ enrichment of each treatment was calculated according to their relative area contribution, assuming that the area-weighted mean $^{15}N$ enrichment likely reflects the mass-weighted $^{15}N$ enrichment of bulk scale analyses such as IRMS. We computed Euclidean distance maps according to the resin-filled pore distribution providing a distance into the soil matrix (Supplementary Figs. 4e and f). The $^{15}N$ enrichment of the enriched segments was plotted across the distance into the soil matrix, and hexagonal binning was used to display the number of data points as a heat map using the ggplot package in R.

### 2.6. Cryo-FIB SEM-EDX analysis

Cryogenic scanning electron microscopy (SEM) with electron dispersive X-ray (EDX) spectroscopy analyses were conducted using a TFS/FEI Strata 400 STEM DualBeam FIB (Thermo Fisher Scientific, Waltham, MA) equipped with a Quorum PP3010T Cryo-FIB/SEM Preparation System (Laughton, East Sussex, UK). Microaggregates were separated by dry sieving with a 53-μm sieve. Aggregates were hydrated slowly (~12 h period) after distribution on glass fiber filter paper (Whatman GF/A) using an ultrasonic humidifier at its lowest setting (SPT Ultrasonic Humidifier, Sunpentown, Inc., CA) (Ultrasonic Humidifier, Sunpentown, CA) (Kinyangi et al., 2006). Aggregates were transferred to SEM carbon adhesive tape, rapidly frozen in slush nitrogen, and transferred to the FIB instrument under cryogenic conditions (approximately −165 °C) (transfer details published in Zachman et al. (2016)). Before imaging and milling, samples were sputter-coated using a gold-palladium alloy (10 s at 10 mA). SEM images and EDX maps were collected before and after the sequential removal of approximately 1 μm-thick sections of the aggregate by FIB milling using an ion beam voltage of 30 kV with varying currents (between approximately 5 pA and 500 pA). SEM-EDX images and maps for each aggregate slice were collected at 5 kV and 1.6 nA.

## 3. Results

### 3.1. Greater spatial distribution increases C persistence in clay-rich subsoils

In the subsoil at a depth of 0.8–0.9 m (Supplementary Fig. 1, Supplementary Table 1), the added distributed OM had significantly higher persistence (i.e., lower mineralization) and higher mineral association compared to the hotspot OM (Fig. 1). The cumulative mineralization of the added OM after 50 days of incubation was reduced by 17% when it was distributed compared to the OM added as a hotspot (Fig. 1a). In the first 20 days, the daily mineralization of the distributed OM showed a lower and delayed peak of mineralization, occurring three days later (Fig. 1b). During the peak of the hotspot OM mineralization, the mineralization of the distributed OM was still 74% lower (Fig. 1b).

Analyzing the retained C in the soil after the incubation period, we observed that significantly more distributed OM was converted into mineral-associated OM (heavy fraction) than the hotspot OM (Fig. 1c). The distribution of the OM alone increased the C retention in the heavy fraction by 10% (difference between hotspot and distributed DOM, $p < 0.05$). On the other hand, less than 1% of the added C was recovered as a light fraction (also described as particulate organic matter) for both spatial distributions in this clay-rich subsoil. On average, 42% of the added distributed OM was respired, 0.1% recovered in the light fraction, and 46% recovered in the heavy fraction. These values for the hotspot OM were 50%, 0.4%, and 36%, respectively.

Through microscale observations of cross-sectioned aggregates using

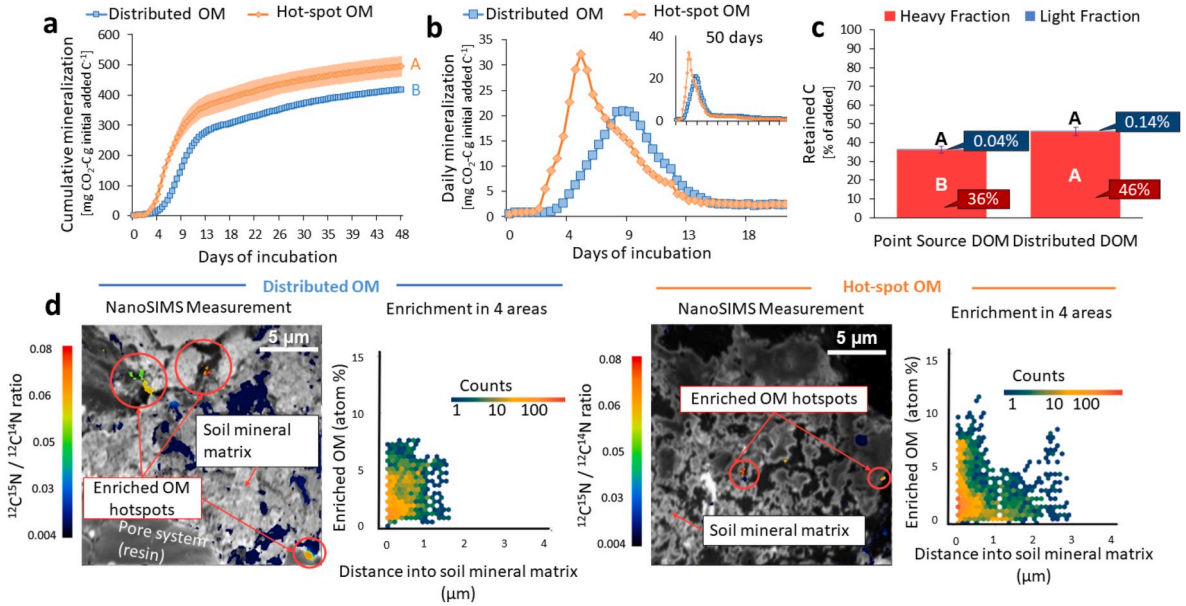


**Fig. 1. Mineralization and mineral association of organic matter (OM) influenced by its spatial distribution in a clay-rich subsoil.** **A** Cumulative mineralization rates of the added OM-derived $CO_2$–C during the 50 days of incubation. **B** Daily mineralization of the OM-derived $CO_2$–C during the first 20 days of incubation. **C** Conversion of the OM-derived C into soil organic matter density fractions post-incubation: mineral-associated organic matter represented by the heavy fraction (>1.8 g $cm^{-3}$) and particulate organic matter represented by the light fraction (<1.8 g $cm^{-3}$) in three jar replicates. Means followed by the same letter do not differ among amendments at $p < 0.05$ (LSD test). **D** $^{15}N$ enrichment of the OM treatments based on $^{12}C^{15}N/^{12}C^{14}N$ ratios calculated from the NanoSIMS measurement (natural abundance = 0.0037) overlaying the $^{16}O^-$ secondary ion signal (greyscale) and $^{15}N$ enrichment ($^{12}C^{15}N/(^{12}C^{15}N + ^{12}C^{14}N)$) quantified in four measurements based on the distance traveled from the pore-mineral interface in direction to the interior of the mineral matrix.

NanoSIMS, we observed hot spots of the added isotopically enriched OM associated with the soil mineral matrix (Fig. 1d). $^{15}$N-enriched OM was tracked in these images since the $^{13}$C levels were too low to be observed. Hotspots of $^{15}$N were overall more enriched for the hotspot OM than the distributed OM in the four areas (field of view of 30 × 30 μm) analyzed on the sectioned aggregate (Fig. 1d). The enrichment levels of OM hotspots were often found to be above five atom percentage (at%) ($^{12}C^{15}N/(^{12}C^{14}N + ^{12}C^{15}N)$ *100), which is close to the enrichment level of the added material (8 at%, Supplementary Fig. 2). We also observed that the hotspot OM traveled further into the soil mineral matrix (Fig. 1d) than the distributed OM. This difference could indicate the saturation of adsorption surfaces in the soil mineral matrix, forcing the OM to move further in the search for new adsorption sites.

### 3.2. Spatial distribution alone plays a lesser role in OM persistence in C-rich topsoil

The effect of the spatial distribution of the added OM seems to play a lesser role in its mineralization and mineral association in the C-rich organic topsoil than in the C-poor subsoil (Fig. 2). We did not observe a significant difference between the cumulative mineralization of the distributed and hotspot OM in the topsoil (Fig. 2a). The daily mineralization in the first 20 days did not present a difference in the peak of mineralization in the OM-rich topsoil as seen for the clay-rich subsoil (Fig. 2b). The peak of mineralization of the distributed OM was sharp (increase and decrease occurring within 24 h) and decreased rapidly on the first day of incubation. On the other hand, the hotspot OM had a lower initial mineralization peak but decreased slower during the first five days of incubation. Analyzing the C retention in the soil after the incubation, we found that due to the OM-rich composition of this soil (Supplementary Fig. 1), a greater proportion of the added OM was retained in the particulate organic matter fraction (Fig. 2c). We did not observe a significant difference in the C retention in both fractions between the hotspot and distributed OM for the OM-rich topsoil (Fig. 2c). Averaging the two OM treatments, 60% of the added OM in the topsoil was respired. In contrast, 25% was recovered in the light fraction and 4% in the heavy fraction.

At the microscale, we observed fewer $^{15}$N-enriched spots in the regions analyzed across the sectioned aggregate than in the clay-rich subsoil (Fig. 2d). For the hotspot OM, enrichment levels were overall not higher than 1 at% in the four spots analyzed. For the distributed OM, no $^{15}$N enrichment was found, mainly due to this topsoil's high OM content (mostly light fraction) (Supplementary Fig. 1), making the $^{15}$N less detectable NanoSIMS due to a dilution effect of the enrichment.

## 4. Discussion

### 4.1. Mechanisms of OM persistence in top and subsoil depths according to the microscale spatial distribution

Here we demonstrate that the greater spatial distribution of the added distributed OM in the clay-rich subsoil significantly increased its persistence in the soil system, but the effect of this spatial distribution is lower in the highly organic topsoil. In Fig. 4, we illustrate the two main proposed reasons for the observed OM persistence depending on their spatial distribution in clay-rich subsoils compared to topsoil rich in particulate OM. The significantly higher cumulative mineralization rates of the hotspot OM (Fig. 1a) suggest a higher specialization of the decomposer microorganisms (Mechanism 1, Fig. 4). Because decomposer microorganisms aim to obtain maximum efficiency in metabolic investment, they maximize enzyme production where the substrate is more concentrated (Dekel and Alon, 2005). The high enrichment of $^{15}$N in single spots of OM found in the NanoSIMS analyses for the hotspot OM illustrates the heterogeneous arrangement of this substrate in the soil (Fig. 1d). Therefore, the presence of a hotspot of C in the soil matrix could enhance mineralization and decrease the formation of mineral interactions, as observed by the lower OM recovery in the heavy mineral fraction (Fig. 1c).

On the other hand, the distributed OM was easily separated from these decomposers due to the greater microscale spatial distribution (Mechanism 2, Fig. 2). Due to the highly heterogeneous soil environment, the distributed OM will likely occur less concentrated for the

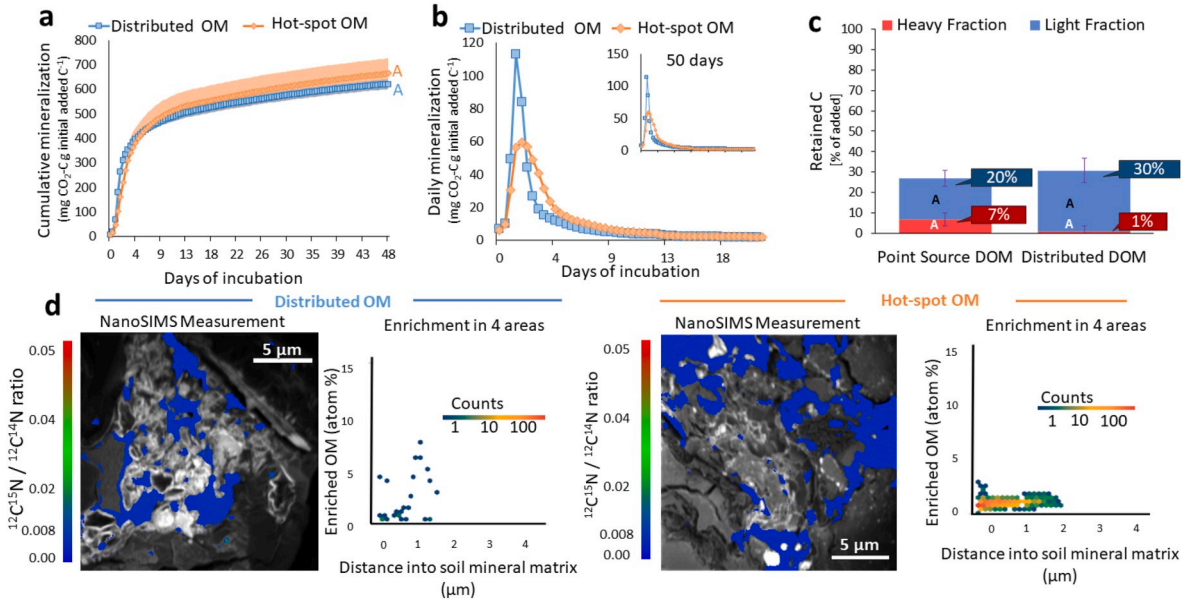


**Fig. 2. Decomposition and mineral association of organic matter (OM) influenced by its spatial distribution in organic matter-rich topsoil.** **A** Cumulative mineralization rates of the added OM-derived $CO_2$–C during the 50 days of incubation. **B** Daily mineralization of the OM-derived $CO_2$–C during the first 20 days of incubation. **C** Conversion of the OM-derived C into soil organic matter density fractions post-incubation: mineral-associated organic matter represented by the heavy fraction (>1.8 g cm$^{-3}$) and particulate organic matter represented by the light fraction (<1.8 g cm$^{-3}$). Means followed by the same letter do not differ among amendments at $p < 0.05$ (LSD test). **D** $^{15}$N enrichment of the OM treatments based on $^{12}C^{15}N/^{12}C^{14}N$ ratios calculated from the NanoSIMS measurement (natural abundance = 0.0037) overlaying the $^{16}O^-$ secondary ion signal (greyscale) and $^{15}$N enrichment ($^{12}C^{15}N/(^{12}C^{15}N + ^{12}C^{14}N)$) quantified in four measurements based on the distance traveled from the pore-mineral interface in direction to the interior of the mineral matrix.

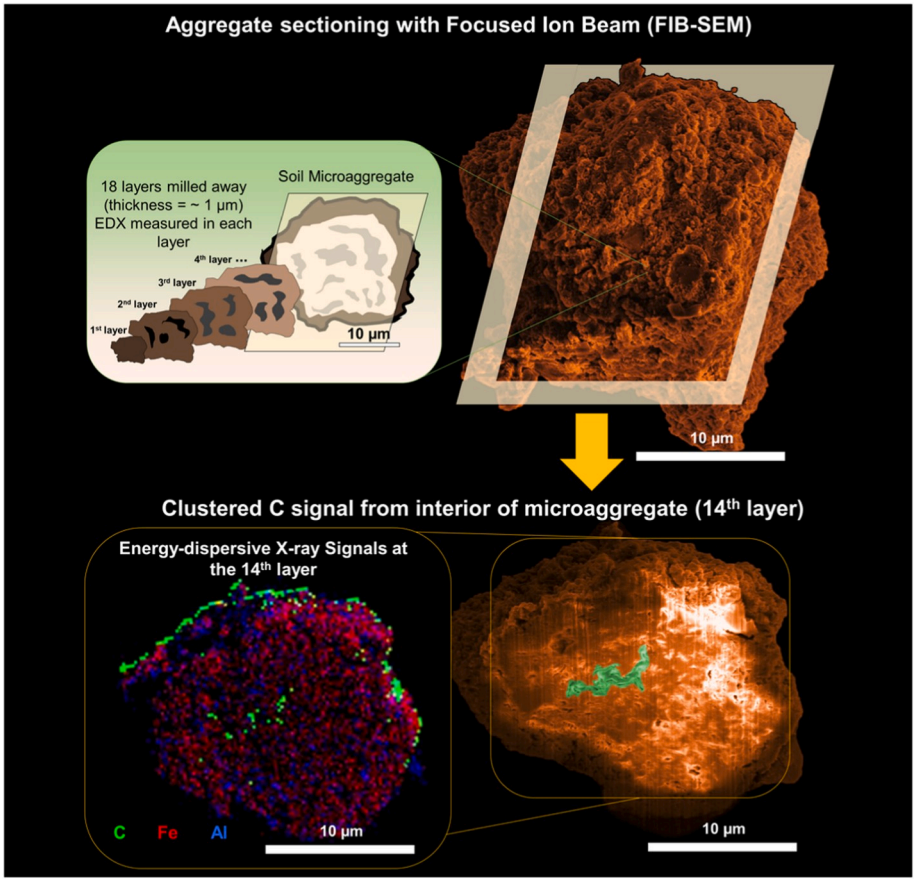


**Fig. 3. Identification of clustered C inside a topsoil microaggregate by cryo-FIB/EDX**. Composite 3D image showing Fe, Al, and C distribution in a layer of a sectioned topsoil microaggregate measured by energy-dispersive X-ray spectroscopy (EDX) demonstrates that mineral interactions can play an essential role in clay-rich microaggregates from topsoil layers rich in organic matter light fractions. Note that the carbon on the particle exterior is only visible on the upper-right side due to detector shadowing, and this surface carbon may not be inherent to the material (e.g., deposited during sample handling/preparation). The C clustered in the interior of the microaggregate was highlighted in green color in the SEM image. A fully animated version of the 3D data is available in supplementary materials. (For interpretation of the references to color in this figure legend, the reader is referred to the Web version of this article.)

decomposers (i.e., dilution). Lower concentrations of a substrate are known to limit mineralization (German et al., 2011), explaining the lower cumulative mineralization of the distributed OM (Fig. 1a). Also, Andisols are recognized for their high binding effect on soil mineral surfaces (Asano and Wagai, 2014), which potentially enhanced the distributed OM conversion into mineral-associated OM (Fig. 1c) and contributed to reducing the microbial accessibility (Fig. 1a and b). These volcanic-ash soils, taxonomically Andisols (Soil Survey Staff, 2010), are ideal for examining organo-mineral associations occurring at a smaller spatial scale due to the high presence of short-range-order (SRO) minerals compared to other soils (Dahlgren et al., 2004; Asano and Wagai, 2014). They are also recognized for their enhanced C storage capacity, making them a vital soil group worldwide (Zieger et al., 2018). The observations at the nanoscale in Andisols highlight the importance of weathering silicate phases in stabilizing OM. However, these processes are not unique to this soil group as they occur in other soil types (Basile-Doelsch et al., 2015). Therefore, the results observed in our study are applicable, but not restricted, to this soil class. The high recovery of the added C as a heavy fraction in the subsoil and the almost absence of $^{13}C$ recovered as light fraction (Fig. 1) indicates interactions of a large proportion of the OM inputs with mineral surfaces. We recognize that microorganisms have likely decomposed the added inputs before being bound to the soil minerals, as most of the persistent OC has likely first passed through microbial biomass (Benner R., 2011; Cotrufo et al., 2013; Liang et al., 2019). In a global evaluation, Georgiou et al. (2022) reported that subsoil saturation levels of mineral surfaces are only 20%, representing the great potential for increasing C stocks. Therefore, our study emphasizes the potential of subsoils in promoting greater C persistence through organo-mineral associations.

In a similar experiment, Shi et al. (2021a) observed lower microbial activity (measured by heat dissipation) as a result of more concentrated glucose additions (i.e., hotspot addition) compared to more distributed additions in topsoil (0.05–0.15 m) collected from a Cambisol with a sandy loam texture during a 50-h incubation. According to the authors, large microorganism colonies can grow in hotspot substrates, but they are more limited to these hot spots. On the other hand, according to these authors, more distributed substrates can be colonized in multiple locations, which results in higher microbial activity. Likewise, Portell et al. (2018), using modeling techniques, highlighted that the likelihood for microbes to assimilate an organic substrate is lower when distributed in an aggregated pattern than in a more distributed pattern (Portell et al., 2018). These findings follow our observation in the topsoil, where the mineralization peak was higher for the distributed DOM during the first days of incubation (Fig. 2b). However, we observed that these differences had a minor influence on the overall OM persistence, given the similar cumulative mineralization after 50 days (Fig. 2a) and consistent with the similar amount of OM retained in each fraction after the incubation period (Fig. 2c). We observed contrasting trends in the clay-rich subsoil (Fig. 1), suggesting that microbial responses to OM distribution depend highly on soil depth.

Here we demonstrated with experimental data that the spatial distribution of OM significantly impacts its persistence in soils and that this influence is highly dependent on soil depth and amounts as well as forms of OM. Our results suggest that promoting a wider spatial distribution of OM in subsoils can significantly foster its persistence, while the spatial distribution of OM plays a lesser effect in topsoils rich in particulate OM. Subsoils are recognized in OC storage since they often represent more than half of the total soil OC stock (Rumpel and Kögel-Knabner, 2010). Also, several reports have highlighted the underestimated importance of belowground inputs for C sequestration in soil systems (Pollierer et al., 2007; Taghizadeh-Toosi et al., 2016; Sokol and Bradford, 2019). Therefore, our results contribute to our understanding of long-term OM persistence.

It is important to emphasize that although we have focused on

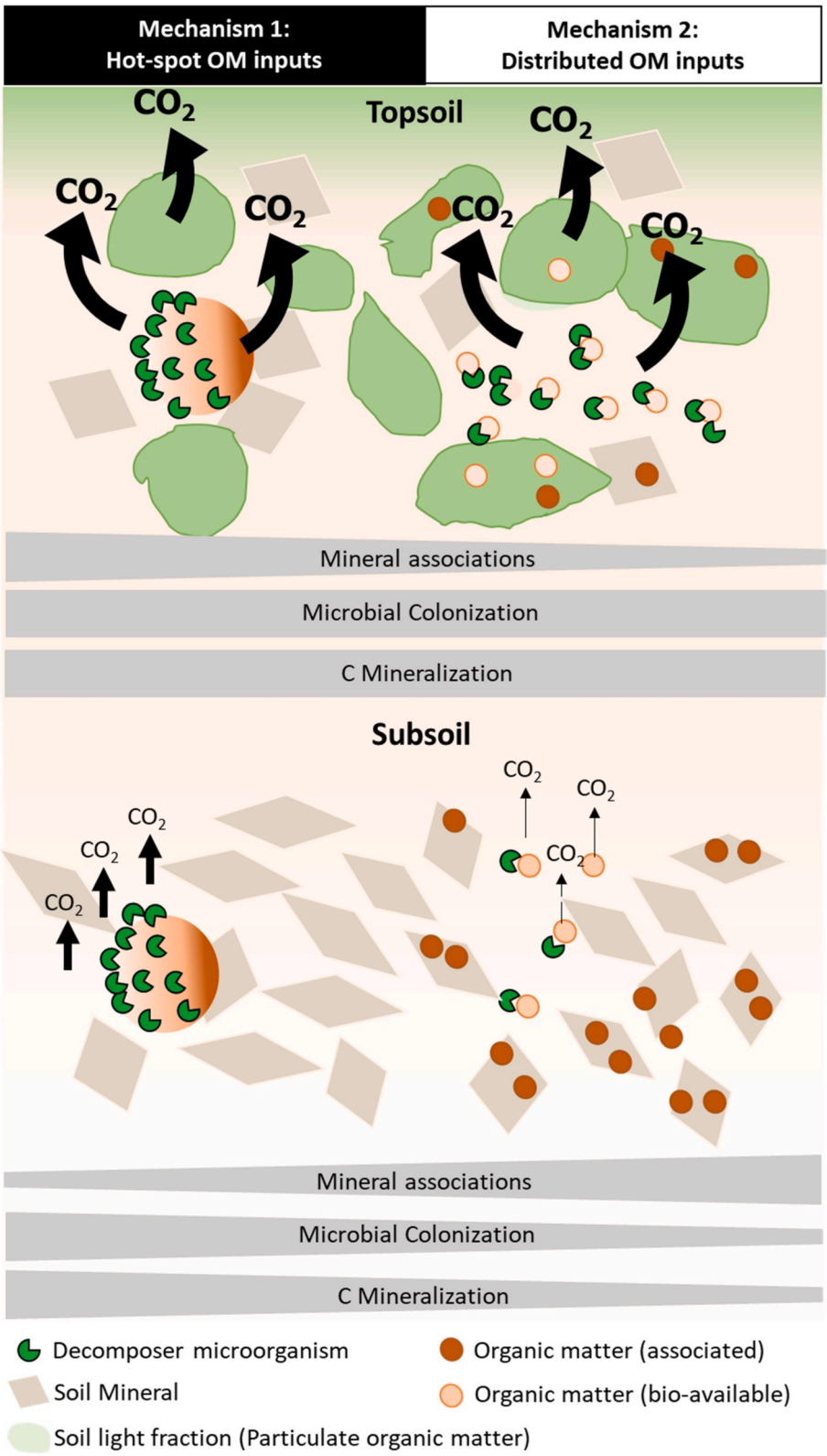


**Fig. 4. Proposed mechanisms for mineralization and stabilization of hotspot and distributed organic matter inputs in topsoil and subsoil**. The Figure illustrates how the spatial distribution of organic matter inputs mediates interactions among decomposer microorganisms, the soil light fraction, and soil minerals.

evaluating the effect of microscale spatial distribution and soil depth, other factors, such as pore space and moisture contents, are essential (Schlüter et al., 2018). We encourage future experimental studies evaluating the effects of the spatial distribution of OM substrates for microbial breakdown combined with different factors, especially related to differences in spatial architecture driven by soil texture and mineral properties.

### 4.2. Higher proportions of particulate organic matter in topsoil overrule the effect of spatial distribution

We observed that the spatial distribution of the added OM had a minor impact on its mineralization in the highly organic topsoil compared to the clay-rich subsoil. Due to the high OM contents in the topsoil, the decomposing microorganisms have access to more substrate than in the clay-rich subsoil. The high proportion of OC associated with the light fraction may be explained by the soil samples collected from a forest area composed of an o'hia and mixed fern vegetation (hapu'u – *Cybotium* spp.- and uluhe – *Dicronopteris linearis* Burm.). Therefore, regardless of their spatial distribution, any OM inputs were mineralized to an equal extent by the microbial community, as both OM inputs showed the same cumulative mineralization rates (Fig. 2a). Moreover, the 10% higher association of the distributed OM with the soil light fraction (Fig. 2c) shows that distributed OM may be easily intercepted by the soil particulate OM, reducing contact with soil minerals. The added OM's mineralization was higher overall in the topsoil, mostly due to a lower proportion of OC associated with the mineral fraction than in the subsoil (Supplementary Fig. 1).

Nonetheless, binding to the light fraction seems to perform an important role in preventing the OM from mineralization as it preserved 20% of the added C throughout the incubation period (Fig. 2). We did not observe significant differences in the mineral-associated OC (Fig. 2c) despite the higher $^{15}N$ enrichment observed in the NanoSIMS for the hotspot OM (Fig. 2d). Since these differences were not significant, we can argue that this effect of spatial distribution on organo-mineral interactions was overall minor in this topsoil. The low amount of mineral-associated C fractions in this soil compared to organic fractions such as fPOM and oPOM (Supplementary Fig. 1) is likely the reason for the low recovery of the added C in organo-mineral fractions. As the C mineralization from native SOC did not differ between amended and control soils, priming effects did not present a significant role in these topsoil samples.

To illustrate the presence of naturally occurring hotspot C in the mineral fraction of the high-organic topsoil, we performed a 3-dimensional assessment of the C distribution. We used energy-dispersive X-ray spectroscopy (EDX) combined with successive sectioning of a clay-rich microaggregate (~20 μm-diameter) in a non-incubated sample by cryogenic focused ion beam (cryo-FIB) (Fig. 3, Supplementary Video). While elements such as Fe and Al were relatively homogeneously distributed in the interior of the observed soil aggregate, the C signal was clustered on the micron scale, consistent with a hotspot of OM. As shown by $^{13}C$ nuclear magnetic resonance spectroscopy (NMR) (Supplementary Fig. 3), the similar proportion of C groups between the topsoil OM light fraction (e.g., hotspot particulate OM) and heavy fraction supports the notion that hotspot OM may accrue in the heavy fraction through mechanisms such as aggregation and mineral associations (Kögel-Knabner et al., 2008; Totsche et al., 2018). Therefore, although the spatial distribution of OM had a minor impact on its mineralization and retention in this highly organic topsoil, the observation of the spatial distribution of OM at the microscale can bring essential insights into the mechanisms responsible for OM persistence.

## 5. Conclusions

We experimentally manipulated the microscale spatial distribution of OM inputs in top and subsoil depths by adding contrasting arrangements of dissolved organic matter: hotspot and distributed. The spatial distribution of the organic matter significantly affected its persistence, especially in clay-rich subsoils. The effect of spatial distribution alone decreased the cumulative mineralization of the added C by 17% and increased its conversion to mineral-associated OM by 10%. This influence of spatial distribution is diminished in the highly organic topsoil, likely due to the higher proportions of low-density fractions of particulate OM. Image analysis using NanoSIMS and FIB-SEM confirmed our observations in the bulk soil, illustrating both spatial distributions inside of soil aggregates. Overall, our experiment emphasizes the role of substrate microscale spatial heterogeneity on soil microbial communities and organic matter persistence. We demonstrated that depth-related changes, such as soil mineralogy especially influence this effect.

## Declaration of competing interest

The authors declare that they have no known competing financial interests or personal relationships that could have appeared to influence the work reported in this paper.

## Data availability

Data will be made available on request.

## Acknowledgments

The Technical University of Munich Institute for Advanced Study provided funding for this study. MJZ and LFK acknowledge support by the NSF (DMR-1654596) and Packard Foundation. This work used the Cornell Center for Materials Research Shared Facilities supported through the NSF MRSEC program (DMR-1719875). Additional support for the FIB/SEM cryo-stage and transfer system was provided by the Kavli Institute at Cornell (KIC) for Nanoscale Science and the Energy Materials Center at Cornell, DOE EFRC BES (DE-SC0001086). The FEI Titan Themis 300 was acquired through NSF-MRI-1429155, with additional support from Cornell University, the Weill Institute, and the KIC. The authors thank Katherine E. Grant and Louis A. Derry (Cornell University Earth and Atmospheric Sciences) for providing soil samples from the Polulu Flow, HI. The authors thank Akio Enders and Kelly Hanley for their technical support.

## Appendix A. Supplementary data

Supplementary data to this article can be found online at https://doi.org/10.1016/j.soilbio.2022.108921.

## References

Abu-Ashour, J., Joy, D.M., Lee, H., Whiteley, H.R., Zelin, S., 1994. Transport of microorganisms through soil. Water, Air, and Soil Pollution 75, 141–158.
Asano, M., Wagai, R., 2014. Evidence of aggregate hierarchy at micro- to submicron scales in an allophanic Andisol. Geoderma 216, 62–74.
Babey, T., Vieublé-Gonod, L., Rapaport, A., Pinheiro, M., Garnier, P., De Dreuzy, J.-R., 2017. Spatiotemporal simulations of 2, 4-D pesticide degradation by microorganisms in 3D soil-core experiments. Ecological Modelling 344, 48–61.
Basile-Doelsch, I., Balesdent, J., Rose, J., 2015. Are interactions between organic compounds and nanoscale weathering minerals the key drivers of carbon storage in soils? Environmental Science and Technology 49, 3997–3998.
Baumert, V.L., Vasilyeva, N.A., Vladimirov, A.A., Meier, I.C., Kogel-Knabner, I., Mueller, C.W., 2018. Root exudates induce soil macroaggregation facilitated by fungi in subsoil. Frontiers in Environmental Science 6, 140.
Baveye, P.C., Otten, W., Kravchenko, A., Balseiro-Romero, M., Beckers, E., Chalhoub, M., Darnault, C., Eickhorst, T., Garnier, P., Hapca, S., Kiranyaz, S., Monga, O., Mueller, C.W., Nunan, N., Pot, V., Schluter, S., Schmidt, H., Vogel, H.J., 2018. Emergent properties of microbial activity in heterogeneous soil microenvironments: different research approaches are slowly converging, yet major challenges remain. Frontiers in Microbiology 9, 1929.
Benner, R., 2011. Biosequestration of carbon by heterotrophic microorganisms. Nature Reviews Microbiology 9, 75.
Besnard, E., Chenu, C., Balesdent, J., Puget, P., Arrouays, D., 1996. Fate of particulate organic matter in soil aggregates during cultivation. European Journal of Soil Science 47, 495–503.
Castellano, M.J., Mueller, K.E., Olk, D.C., Sawyer, J.E., Six, J., 2015. Integrating plant litter quality, soil organic matter stabilization, and the carbon saturation concept. Global Change Biology 21, 3200–3209.
Cotrufo, M.F., Wallenstein, M.D., Boot, C.M., Denef, K., Paul, E., 2013. T he Microbial Efficiency-Matrix Stabilization (MEMS) framework integrates plant litter decomposition with soil organic matter stabilization: do labile plant inputs form stable soil organic matter? Global Change Biology 19, 988–995.
Dahlgren, R.A., Saigusa, M., Ugolini, F.C., 2004. The nature, properties and management of volcanic soils. Advances in Agronomy 82 82, 113–182.

DeCiucies, S., Whitman, T., Woolf, D., Enders, A., Lehmann, J., 2018. Priming mechanisms with additions of pyrogenic organic matter to soil. Geochimica et Cosmochimica Acta 238, 329–342.
Dekel, E., Alon, U., 2005. Optimality and evolutionary tuning of the expression level of a protein. Nature 436, 588–592.
Ebrahimi, A., Or, D., 2018. Dynamics of soil biogeochemical gas emissions shaped by remolded aggregate sizes and carbon configurations under hydration cycles. Global Change Biology 24, e378–e392.
Falconer, R.E., Battaia, G., Schmidt, S., Baveye, P., Chenu, C., Otten, W., 2015. Microscale heterogeneity explains experimental variability and non-linearity in soil organic matter mineralisation. PLoS One 10, e0123774.
Georgiou, K., Jackson, R.B., Vindušková, O., Abramoff, R.Z., Ahlström, A., Feng, W., Harden, J.W., Pellegrini, A.F.A., Polley, H.W., Soong, J.L., Riley, W.J., Torn, M.S., 2022. Global stocks and capacity of mineral-associated soil organic carbon. Nature Communications 13, 3797.
German, D.P., Chacon, S.S., Allison, S.D., 2011. Substrate concentration and enzyme allocation can affect rates of microbial decomposition. Ecology 92, 1471–1480.
Golchin, A., Oades, J.M., Skjemstad, J.O., Clarke, P., 1994. Soil-structure and carbon cycling. Australian Journal of Soil Research 32, 1043–1068.
Gormanns, P., Reckow, S., Poczatek, J.C., Turck, C.W., Lechene, C., 2012. Segmentation of multi-isotope imaging mass spectrometry data for semi-automatic detection of regions of interest. PLoS One 7, e30576.
Grant, K.E., Galy, V.V., Chadwick, O.A., Derry, L.A., 2019. Thermal oxidation of carbon in organic matter rich volcanic soils: insights into SOC age differentiation and mineral stabilization. Biogeochemistry 144, 291–304.
Inagaki, T.M., Possinger, A.R., Grant, K.E., Schweizer, S.A., Mueller, C.W., Derry, L.A., Lehmann, J., Kogel-Knabner, I., 2020. Subsoil organo-mineral associations under contrasting climate conditions. Geochimica et Cosmochimica Acta 270, 244–263.
Kinyangi, J., Solomon, D., Liang, B., Lerotic, M., Wirick, S., Lehmann, J., 2006. Nanoscale biogeocomplexity of the organomineral assemblage in soil: application of STXM microscopy and C 1s-NEXAFS spectroscopy. Soil Science Society of America Journal 70, 1708–1718.
Knicker, H., Ludemann, H.D., 1995. N-15 and C-13 CPMAS and solution NMR studies of N-15 enriched plant material during 600 days of microbial degradation. Organic Geochemistry 23, 329–341.
Kögel-Knabner, I., Amelung, W., 2020. Soil organic matter in major pedogenic soil groups. Geoderma 384, 114785.
Kögel-Knabner, I., Guggenberger, G., Kleber, M., Kandeler, E., Kalbitz, K., Scheu, S., Eusterhues, K., Leinweber, P., 2008. Organo-mineral associations in temperate soils: integrating biology, mineralogy, and organic matter chemistry. Journal of Plant Nutrition and Soil Science 171, 61–82.
Kramer, M.G., Sanderman, J., Chadwick, O.A., Chorover, J., Vitousek, P.M., 2012. Long-term carbon storage through retention of dissolved aromatic acids by reactive particles in soil. Global Change Biology 18, 2594–2605.
Kuka, K., Franko, U., Ruhlmann, J., 2007. Modelling the impact of pore space distribution on carbon turnover. Ecological Modelling 208, 295–306.
Kuzyakov, Y., Blagodatskaya, E., 2015. Microbial hotspots and hot moments in soil: concept & review. Soil Biology and Biochemistry 83, 184–199.
Lal, R., Smith, P., Jungkunst, H.F., Mitsch, W.J., Lehmann, J., Nair, P.K.R., McBratney, A. B., Sa, J.C.D., Schneider, J., Zinn, Y.L., Skorupa, A.L.A., Zhang, H.L., Minasny, B., Srinivasrao, C., Ravindranath, N.H., 2018. The carbon sequestration potential of terrestrial ecosystems. Journal of Soil and Water Conservation 73, A145–A152.
Lavkulich, L., 1981. Methods Manual, Pedology Laboratory. University of British Columbia, Department of Soil Science, Vancouver, BC, CA.
Lehmann, J., Hansel, C.M., Kaiser, C., Kleber, M., Maher, K., Manzoni, S., Nunan, N., Reichstein, M., Schimel, J.P., Torn, M.S., Wieder, W.R., Kogel-Knabner, I., 2020. Persistence of soil organic carbon caused by functional complexity. Nature Geoscience 13, 529–534.
Liang, C., Amelung, W., Lehmann, J., Kastner, M., 2019. Quantitative assessment of microbial necromass contribution to soil organic matter. Global Change Biology 25, 3578–3590.
Lowery, B., Hickey, W.J., Arshad, M.A., Lal, R., 1997. Soil Water Parameters and Soil Quality, Methods for Assessing Soil Quality, pp. 143–155.
Marin-Spiotta, E., Chadwick, O.A., Kramer, M., Carbone, M.S., 2011. Carbon delivery to deep mineral horizons in Hawaiian rain forest soils. Journal of Geophysical Research-Biogeosciences 116.
Marschner, B., Kalbitz, K., 2003. Controls of bioavailability and biodegradability of dissolved organic matter in soils. Geoderma 113, 211–235.
Marschner, P., Marhan, S., Kandeler, E., 2012. Microscale distribution and function of soil microorganisms in the interface between rhizosphere and detritusphere. Soil Biology and Biochemistry 49, 174–183.
Mehra, O., Jackson, M., 1958. Iron oxide removal from soils and clays by a dithionite-citrate system buffered with sodium bicarbonate. National Conference on Clays and Clay Minerals 317–327.
Mueller, C.W., Weber, P.K., Kilburn, M.R., Hoeschen, C., Kleber, M., Pett-Ridge, J., 2013. Advances in the analysis of biogeochemical interfaces: NanoSIMS to investigate soil microenvironments. Advances in Agronomy 121 121, 1–46.
Nunan, N., Leloup, J., Ruamps, L.S., Pouteau, V., Chenu, C., 2017. Effects of habitat constraints on soil microbial community function. Scientific Reports 7, 4280.
Nunan, N., Schmidt, H., Raynaud, X., 2020. The ecology of heterogeneity: soil bacterial communities and C dynamics. Philosophical Transactions of the Royal Society B 375, 20190249.
Ostertag, R., Cordell, S., Michaud, J., Cole, T.C., Schulten, J.R., Publico, K.M., Enoka, J. H., 2009. Ecosystem and restoration consequences of invasive woody species removal in Hawaiian lowland wet forest. Ecosystems 12, 503–515.
Pollierer, M.M., Langel, R., Korner, C., Maraun, M., Scheu, S., 2007. The underestimated importance of belowground carbon input for forest soil animal food webs. Ecology Letters 10, 729–736.
Portell, X., Pot, V., Garnier, P., Otten, W., Baveye, P.C., 2018. Microscale heterogeneity of the spatial distribution of organic matter can promote bacterial biodiversity in soils: insights from computer simulations. Frontiers in Microbiology 9, 1583.
Reynolds, A.M., Dutta, T.K., Curtis, R.H., Powers, S.J., Gaur, H.S., Kerry, B.R., 2010. Chemotaxis can take plant-parasitic nematodes to the source of a chemo-attractant via the shortest possible routes. Journal of The Royal Society Interface 8, 568–577.
Rumpel, C., Kögel-Knabner, I., 2010. Deep soil organic matter—a key but poorly understood component of terrestrial C cycle. Plant and Soil 338, 143–158.
Rumpel, C., Lehmann, J., Chabbi, A., 2018. '4 per 1,000'initiative will boost soil carbon for climate and food security. Nature 553, 27-27.
Schlüter, S., Eickhorst, T., Mueller, C.W., 2018. Correlative imaging reveals holistic view of soil microenvironments. Environmental Science and Technology 53, 829–837.
Schoeneberger, P.J., Wysocki, D.A., Benham, E.C., 2012. Field Book for Describing and Sampling Soils. Government Printing Office.
Schweizer, S.A., Hoeschen, C., Schluter, S., Kogel-Knabner, I., Mueller, C.W., 2018. Rapid soil formation after glacial retreat shaped by spatial patterns of organic matter accrual in microaggregates. Global Change Biology 24, 1637–1650.
Shi, A., Chakrawal, A., Manzoni, S., Fischer, B.M., Nunan, N., Herrmann, A.M., 2021a. Substrate spatial heterogeneity reduces soil microbial activity. Soil Biology and Biochemistry 152, 108068.
Shi, A.D., Chakrawal, A., Manzoni, S., Fischer, B.M.C., Nunan, N., Herrmann, A.M., 2021b. Substrate spatial heterogeneity reduces soil microbial activity. Soil Biology and Biochemistry 152, 108068.
Silva, J.H.S., Deenik, J.L., Yost, R.S., Bruland, G.L., Crow, S.E., 2015. Improving clay content measurement in oxidic and volcanic ash soils of Hawaii by increasing dispersant concentration and ultrasonic energy levels. Geoderma 237, 211–223.
Soil Survey Staff, 2010. Keys to Soil Taxonomy, eleventh ed. Department of Agriculture: Natural Resources Conservation Service.
Sokol, N.W., Bradford, M.A., 2019. Microbial formation of stable soil carbon is more efficient from belowground than aboveground input. Nature Geoscience 12, 46–53.
Sommer, C., Straehle, C., Koethe, U., Hamprecht, F.A., 2011. Ilastik: Interactive Learning and Segmentation Toolkit, 2011 IEEE International Symposium on Biomedical Imaging: from Nano to Macro. IEEE, pp. 230–233.
Taghizadeh-Toosi, A., Christensen, B.T., Glendining, M., Olesen, J.E., 2016. Consolidating soil carbon turnover models by improved estimates of belowground carbon input. Scientific Reports 6, 32568.
Thurman, E.M., 2012. Organic Geochemistry of Natural Waters. Springer Science & Business Media.
Tisdall, J., Oades, J.M., 1982. Organic matter and water-stable aggregates in soils. European Journal of Soil Science 33, 141–163.
Totsche, K.U., Amelung, W., Gerzabek, M.H., Guggenberger, G., Klumpp, E., Knief, C., Lehndorff, E., Mikutta, R., Peth, S., Prechtel, A., Ray, N., Kogel-Knabner, I., 2018. Microaggregates in soils. Journal of Plant Nutrition and Soil Science 181, 104–136.
Van Haastert, P.J., Bosgraaf, L., 2009. Food searching strategy of amoeboid cells by starvation induced run length extension. PLoS One 4, e6814.
Van Veen, J., Kuikman, P., 1990. Soil structural aspects of decomposition of organic matter by microorganisms. Biogeochemistry 11, 213–233.
Vermeulen, S., Bossio, D., Lehmann, J., Luu, P., Paustian, K., Webb, C., Auge, F., Bacudo, I., Baedeker, T., Havemann, T., Jones, C., King, R., Reddy, M., Sunga, I., Von Unger, M., Warnken, M., 2019. A global agenda for collective action on soil carbon. Nature Sustainability 2, 2–4.
Vert, M., Doi, Y., Hellwich, K.H., Hess, M., Hodge, P., Kubisa, P., Rinaudo, M., Schué, F., 2012. Terminology for biorelated polymers and applications (IUPAC Recommendations 2012). Pure and Applied Chemistry 84 (2), 377–410.
Vogel, L., Pot, V., Makowski, D., Garnier, P., Baveye, P., 2018. To what extent do uncertainty and sensitivity analyses help unravel the influence of microscale physical and biological drivers in soil carbon dynamics models? Ecological Modelling 383, 10–22.
Wagai, R., Kajiura, M., Asano, M., 2020. Iron and aluminum association with microbially processed organic matter via meso-density aggregate formation across soils: organo-metallic glue hypothesis. SOIL 6, 597–627.
Wagai, R., Kishimoto-Mo, A.W., Yonemura, S., Shirato, Y., Hiradate, S., Yagasaki, Y., 2013. Linking temperature sensitivity of soil organic matter decomposition to its molecular structure, accessibility, and microbial physiology. Global Change Biology 19, 1114–1125.
Witzgall, K., Vidal, A., Schubert, D.I., Höschen, C., Schweizer, S.A., Buegger, F., Pouteau, V., Chenu, C., Mueller, C.W., 2021. Particulate organic matter as a functional soil component for persistent soil organic carbon. Nature Communications 12, 1–10.
Wolfe, E.W., Morris, J., 1996. Geologic Map of the Island of Hawaii.
Zachman, M.J., Asenath-Smith, E., Estroff, L.A., Kourkoutis, L.F., 2016. Site-specific preparation of intact solid–liquid interfaces by label-free in situ localization and cryo-focused ion beam lift-out. Microscopy and Microanalysis 22, 1338–1349.
Zieger, A., Kaiser, K., Ríos Guayasamín, P., Kaupenjohann, M., 2018. Massive carbon addition to an organic-rich Andosol increased the subsoil but not the topsoil carbon stock. Biogeosciences 15, 2743–2760.